

# Dark Channel Prior Dehazing Combined with Image Quality Assessment Applied to Haze Detection

Chih-Ping Yen \*, Cheng-Tan Tung, Hsin-Hsiung Kao, Chen-Yu Li

**Abstract**—Driving in hazy conditions with low visibility can easily lead to accidents due to delayed reactions. Consequently, integrating image processing techniques into existing traffic CCTV systems offers a cost-effective solution for real-time haze detection and early warning systems. This study develops a novel haze detection model by combining the dark channel prior dehazing algorithm with advanced image quality assessment metrics, ensuring accurate haze degree classification. Experimental results demonstrate that this model combined with the Structural SIMilarity (SSIM) image quality assessment method can effectively capture the changes in luminance, contrast, and structure of haze images to distinguish different haze degrees. Therefore, the performance Accuracy @1 reaches 96.55%. In addition, the correlation coefficients Pearson, Spearman, and Kendall also proved once again that the correlation between the ranking results calculated by SSIM and the actual ranking of haze degrees is the highest. Pearson and Spearman are both 0.9862, and Kendall is 0.9770. Moreover, the proposed model conducts a sensitivity analysis on the local patch size and the transmission parameter  $w$ . The results show that with  $w=1$  and the local patch size is between  $39 \times 39$  and  $47 \times 47$ , the model can capture haze information more effectively and thereby improve performance. Then, the CHIC image database with haze levels was used for practical verification to confirm that the proposed model can indeed detect different haze densities correctly. Finally, we also explore and analyze the results of nighttime haze image detection. In the future, this model can not only be applied to existing CCTV infrastructure for haze concentration monitoring, but can also be further coordinated with other ITS modules.

**Index Terms**—haze detection, dark channel prior dehazing, image quality assessment, Structural SIMilarity (SSIM), Intelligent Transportation System (ITS)

## I. INTRODUCTION

As the seasons change, dense haze becomes a hidden danger for driving. Driving in haze reduces visibility, increasing the risk of accidents due to delayed reactions. Therefore, if the traffic management department can

Manuscript received July 29, 2024; revised January 16, 2025.

Chih-Ping Yen is a Professor of Information Management Department, Central Police University, Taoyuan 333322, Taiwan, ROC (corresponding author, e-mail: peter@mail.cpu.edu.tw).

Cheng-Tan Tung is an Assistant Professor of Information Management Department, Central Police University, Taoyuan 333322, Taiwan, ROC (e-mail: tung@mail.cpu.edu.tw).

Hsin-Hsiung Kao is an Assistant Professor of Information Management Department, Central Police University, Taoyuan 333322, Taiwan, ROC (e-mail: kao@mail.cpu.edu.tw).

Chen-Yu Li is an Assistant Professor of Information Management Department, Central Police University, Taoyuan 333322, Taiwan, ROC (e-mail: cyli@mail.cpu.edu.tw).

widely increase dense fog detectors and provide real-time alarms on road sections prone to haze. It alerts drivers to reduce speed and maintain a safe distance, enhancing road safety. For example, Taiwan's highways are equipped with 65 dense fog detectors. When visibility is detected to be lower than 400 meters, an alarm will be issued [1]. However, the labor and financial costs of building and maintaining these facilities will be a major burden.

At present, the traffic management department has installed real-time CCTV images in some traffic sections to monitor road conditions and vehicle speeds [2], as shown in the publicly available data in Fig. 1. This study aims to apply image processing technology to existing CCTV systems for haze detection. Future results will provide traffic management departments with extremely low costs to add functions to existing CCTV equipment and add warning facilities to road sections.



Fig. 1. Real-time highway traffic conditions and vehicle speed monitoring.

Nighttime CCTV image recognition is a challenging and separate research area. Due to the weak light at night, CCTV images appear low-contrast, blurry and noisy, which makes it difficult to accurately capture and interpret the details in the image, thus affecting its recognition performance. At the same time, there are many different types and intensities of light sources in the night environment, which causes the color of objects in the image to vary, making it more difficult to identify [3]. Therefore, considering the length of the content, we will add a subsection in Section IV to explore and analyze the results of nighttime haze image detection.

The rest of this paper is organized as follows. In the next section, we summarize the related work. Section III presents the proposed haze detection model and explains its processing flow. Sections IV show experimental results and discussion. Finally, Section V concludes the whole paper.

## II. RELATED WORK

## A. Single Image Dehazing

Single image dehazing technology refers to dehazing a haze image alone without relying on multiple images or other additional information. Using single-image dehazing is often based on certain objective reasons, such as the lower computational cost of processing a single image, or practical scenarios where only a single hazy image can be obtained (e.g., real-time CCTV images, aerial images) [4]. He [5] proposed a classic single image dehazing algorithm known as the 'dark channel prior' (DCP), based on the statistical characteristics of haze images. In most non-sky areas, the surrounding area of each pixel usually has an extremely low value, which is called a dark pixel. Based on this prior knowledge, dehazing can be performed. Because the DCP method is quite effective, it is also commonly used in other fields. For example, there is a large amount of dust in the welding process of smart manufacturing, and it is used to obtain clear welding images [6]. Overcome motion blur in high-speed motion scenes [7]. Improve the image quality of underwater shooting [8]. Tan [9] made two observations. One is that clear-sky images have higher contrast than images affected by bad weather, and the other is that changes in atmospheric light depend on the distance between the scene and the observer. From these two observations, the author uses Markov random field to restore the local contrast of hazy images. Zhu [10] proposed a simple prior knowledge of color attenuation to remove haze. This prior knowledge models the scene depth of haze images, and uses supervised learning to restore the depth information, thereby effectively removing haze. Tang [11] demonstrated that dark channel features contain the most information for dehazing tasks. The author synthesized various features of haze into a hazy image and used a random forest for regression model learning. Fuh [12] proposed to estimate atmospheric light and scene transmission based on the smallest image channel and patchless. Then use histogram equalization and image multiplication technology to directly process the entire image to achieve fast and effective haze removal. Cai [13] created DehazeNet, a deep architecture based on CNN for image dehazing. Each layer of it is specially designed to reflect the prior knowledge inherent in image dehazing. Yeh [14] proposed the MSRL-DehazeNet deep learning architecture, which decomposes haze images into basic and detail components, and then leverages multi-scale deep residual learning to remove the haze. Chen [15] proposed the DEA-Net deep learning architecture, which enhances promote feature learning through the detail enhanced attention block (DEAB), thereby improving the dehazing performance. This DEAB consists of detail-enhanced convolution (DEConv) and content-guided attention (CGA).

Although haze removal from a single image has its advantages, the effect will be limited in extreme weather or extremely severe haze conditions. This is because a single image lacks sufficient additional information to accurately estimate the density and distribution of haze, so it is necessary to consider using multiple images or the assistance of other sensors.

## B. Haze Image Model

Atmospheric light refers to the light that is affected by the scattering and absorption of atmospheric gases and particulate matter in the natural environment when sunlight spreads in the air. McCartney [16] proposed a haze image model, such as Equation (1).

$$J(x) = I(x)t(x) + A(1 - t(x)) \quad (1)$$

where  $J(x)$  is the observed haze image,  $I(x)$  is the haze-free image,  $A$  is the atmospheric light, and  $t(x)$  is the transmission. Transmission refers to the degree of light attenuation when passing through a medium, such as haze. It is commonly expressed in the range of 0 to 1. Low transmission means thicker haze. The entire haze image model is represented in Fig. 2.

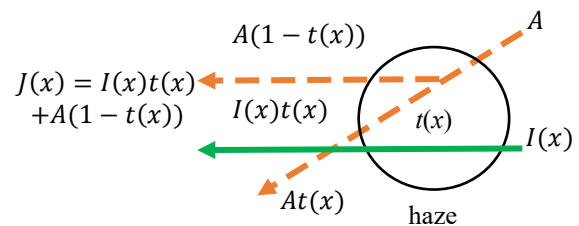


Fig. 2. Haze image model.

## C. Dark Channel Prior Dehazing

He et al. [5] observed a large number of images with haze and found some rules. In a hazy environment, the scenery in some local areas is obscured by haze, causing their brightness in the image to become very low and look blurry or gray. These areas are usually far away from the observer, such as distant mountains and the sky. In areas that are closer to the observer or less affected by haze, the light is not scattered a lot, the brightness is relatively high, and it looks clearer, such as nearby trees, buildings, and the ground. Based on these observations, the author rewrites Equation (1) into Equation (2), and substitutes the estimated values of atmospheric light  $A$  and transmission  $t(x)$  to achieve haze image dehazing.

$$I(x) = \frac{J(x) - A}{t(x)} + A, \quad (2)$$

where  $J(x)$  is the observed image with haze,  $I(x)$  is the image without haze,  $A$  is the atmospheric light, and  $t(x)$  is the transmission. The entire implementation steps are as follows, which is called dark channel prior dehazing.

**Step 1: Obtain dark channel image**

Use Equation (3) to process the surrounding area of each pixel in the haze image and obtain a local minimum on its RGB channel. A new image will be formed, the so-called dark channel image, as shown in Fig. 3.

$$J^{dark}(x) = \min_{y \in \Omega(x)} \left( \min_{c \in \{R, G, B\}} J^c(y) \right), \quad (3)$$

where  $J^c$  represents the  $c$ -th channel of the image, which can be one of the  $R$ ,  $G$ , and  $B$  channels.  $J^{dark}(x)$  is the pixel value of the dark channel image at position  $x$ .  $\Omega(x)$  is a local patch centered on  $x$ , its patch size is usually  $15 \times 15$ , and  $y$  is a

point in the  $\Omega(x)$  patch.

In addition, the author obtained another prior knowledge. He observed that in haze-free images of non-sky types, among all pixels in any local patch (such as  $15 \times 15$ ), the minimum value of the RGB channel is extremely small or tends to 0 ( $J^{dark} \rightarrow 0$ ).

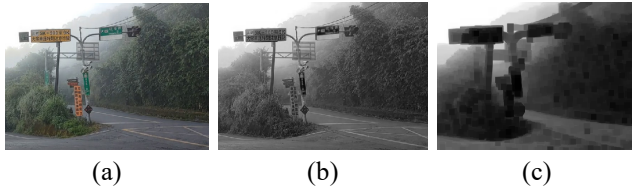


Fig. 3. Dark channel image acquisition. (a) Haze image. (b) Minimum value in RGB channel per pixel. (c) Dark channel image with patch size  $15 \times 15$ .

### Step 2: Estimate atmospheric light

Generally speaking, the non-haze areas in the image have the highest brightness values and can be used as estimated atmospheric light. Therefore, the first 0.1% of the image points with higher pixel values are taken from the dark channel image, and the maximum pixel value is found from the corresponding image point in the original image. Then this maximum pixel value is used as the estimated value of atmospheric light  $A$ .

### Step 3: Calculate the transmission

First, divide both sides of the equal sign of Equation (1) by the estimated atmospheric light value  $A$ , and then perform minimization processing. The result is as shown in Equation (4).

$$\min_{y \in \Omega(x)} \left( \min_{y \in \Omega(x)} \frac{J(x)}{A} \right) = t(x) \min_{y \in \Omega(x)} \left( \min_{y \in \Omega(x)} \frac{I(x)}{A} \right) + 1 - t(x). \quad (4)$$

According to step 1, for haze-free images of non-sky types, the prior knowledge of the dark channel  $J^{dark} \rightarrow 0$  is known, and then the transmission  $t(x)$  is obtained after substituting it into Equation (4). The result is as shown in Equation (5).

$$t(x) = 1 - \min_{y \in \Omega(x)} \left( \min_{y \in \Omega(x)} \frac{J(x)}{A} \right). \quad (5)$$

In addition, the author adds the  $w$  parameter (recommended  $w=0.95$ ) to Equation (5), and then obtains Equation (6), which allows part of the image depth to be retained and avoids excessive dehazing and unnatural scenery.

$$t(x) = 1 - \omega \min_{y \in \Omega(x)} \left( \min_{y \in \Omega(x)} \frac{J(x)}{A} \right). \quad (6)$$

### Step 4: Obtain the dehazed image

Adjust Equation (2) to Equation (7), and substitute the previously known estimated atmospheric light value  $A$  and the transmission  $t(x)$  to obtain the dehazed image, as shown in Fig. 4.

$$I(x) = \frac{J(x) - A}{\max(t(x), t_0)} + A, \quad (7)$$

where  $\max(t(x), t_0)$  is an adjustment made to avoid the

denominator of Equation (2) being 0. By setting  $t_0$  to 0.1, the transmission is guaranteed to be at least 0.1, preventing overly dark or distorted regions in the dehazed image.

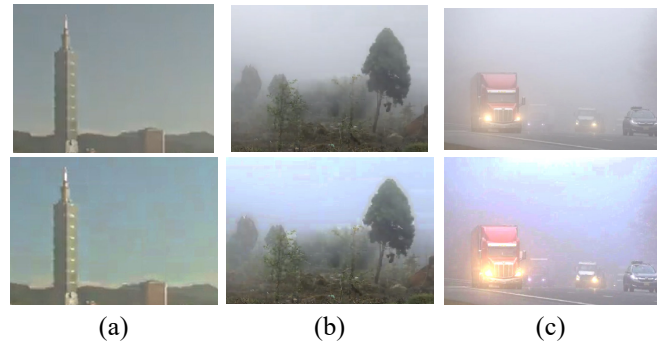


Fig. 4. Haze and haze-free image comparison. (Row 1: Haze images, Row 2: Haze-free images.)

## III. PROPOSED HAZE DETECTION MODEL

This study proposes a haze detection model that integrates advanced image processing techniques into existing CCTV systems, aiming to provide a cost-effective and efficient solution for haze detection. Therefore, we develop a novel haze detection model by combining the dark channel prior dehazing algorithm with advanced image quality assessment metrics, ensuring accurate haze degree classification. As shown in Fig. 5.

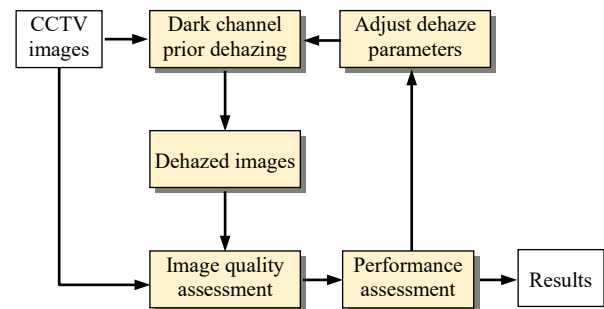


Fig. 5. Proposed haze detection model.

In the proposed model, the dehazed image obtained through dark channel prior dehazing is compared with the original CCTV image to evaluate image quality. The haze degree of the image is then determined based on the image quality assessment results. Therefore, the worse the image quality evaluation results, the more severe the haze. Finally, the performance evaluation results determine which image quality evaluation method is better, and adjust the dehazing parameters to optimize the model performance, thereby achieving the purpose of detection.

### A. Image Quality Assessment

This study evaluates different image quality metrics to identify those most suitable for haze detection in the proposed model.

#### Mean Square Error (MSE)

Equation (8) is used to express the mean square error (MSE) between the original image and the noisy image [17].

$$MSE = \frac{\sum_{i=1}^M \sum_{j=1}^N (I_{ij} - J_{ij})^2}{MN}, \quad (8)$$

where  $I_{ij}$  is the original signal,  $\hat{I}_{ij}$  is the signal with added noise,  $(I_{ij} - \hat{I}_{ij})$  is the noise, and  $M, N$  are the image length and width.

#### Mean Absolute Error (MAE)

Equation (9) is used to express the mean absolute error (MAE) between the original image and the noisy image [17].

$$MAE = \frac{\sum_{i=1}^M \sum_{j=1}^N |I_{ij} - \hat{I}_{ij}|}{MN}, \quad (9)$$

where  $I_{ij}$  is the original signal,  $\hat{I}_{ij}$  represents the noise added to  $I_{ij}$ ,  $(I_{ij} - \hat{I}_{ij})$  is the noise, and  $M, N$  are the image length and width. The difference between MAE and MSE is how they measure error and how they handle error size. Generally speaking, MAE is suitable for situations where the error size is relatively evenly distributed, or is less sensitive to outliers. MSE, on the other hand, gives higher weight to larger errors and so is more sensitive to outliers.

#### Signal to Noise Ratio (SNR)

Signal to Noise Ratio (SNR) [18] describes the ratio of signal strength (signal power) to noise strength (noise power), its unit is decibel (dB), and 1 dB=0.1 bel, such as Equation (10). That is to say, the signal quality is not expressed by the size of the noise, but by the ratio of the useful signal and the noise. When the ratio is large, the human senses will feel that the signal quality is better.

$$\begin{aligned} SNR &= 10 \log_{10} \left( \frac{\text{signal}^2}{\text{noise}^2} \right) \\ &= 10 \log_{10} \left( \frac{\sum_{i=1}^M \sum_{j=1}^N I_{ij}^2}{\sum_{i=1}^M \sum_{j=1}^N (I_{ij} - \hat{I}_{ij})^2} \right), \end{aligned} \quad (10)$$

where  $I_{ij}$  is the original signal,  $\hat{I}_{ij}$  represents the noise added to  $I_{ij}$ ,  $(I_{ij} - \hat{I}_{ij})$  is the noise, and  $M, N$  are the image length and width.

#### Peak Signal to Noise Ratio (PSNR)

The Peak Signal-to-Noise Ratio (PSNR) [19] is a measure of signal quality that uses the peak signal value as a reference. For an 8-bit grayscale image with a range of 0 to 255, the peak signal value is always 255, regardless of the actual pixel values, such as Equation (11).

$$\begin{aligned} PSNR &= 10 \log_{10} \left( \frac{MN 255^2}{\sum_{i=1}^M \sum_{j=1}^N (I_{ij} - \hat{I}_{ij})^2} \right) \\ &= 10 \log_{10} \left( \frac{255^2}{\frac{\sum_{i=1}^M \sum_{j=1}^N (I_{ij} - \hat{I}_{ij})^2}{MN}} \right), \end{aligned} \quad (11)$$

where  $I_{ij}$  is the original signal,  $\hat{I}_{ij}$  represents the noise added to  $I_{ij}$ ,  $(I_{ij} - \hat{I}_{ij})$  is the noise, and  $M, N$  are the image length and width. In addition, the relationship between PSNR and MSE is  $PSNR = 10 \log_{10} (255^2 / MSE)$ .

#### Structural SIMilarity (SSIM) Index

An index to evaluate the similarity of two images, such as Equation (12). The SSIM value is the product of the luminance L, contrast C, and structure S of the two images [20], as shown in Equation (13-15).

$$SSIM(i, j) = L(i, j) C(i, j) S(i, j) \quad (12)$$

$$L(i, j) = \left( \frac{2\mu_i\mu_j + c_1}{\mu_i^2 + \mu_j^2 + c_1} \right), \quad (13)$$

$$C(i, j) = \left( \frac{2\sigma_i\sigma_j + c_2}{\sigma_i^2 + \sigma_j^2 + c_2} \right), \quad (14)$$

$$S(i, j) = \left( \frac{\mu_{ij} + c_3}{\sigma_i\sigma_j + c_3} \right), \quad (15)$$

where  $(i, j)$  denotes the pixel coordinates. By sliding a window, typically of size  $11 \times 11$ , corresponding patches of the two images are extracted and their similarity is calculated. After calculating the similarity of all patches, the average is taken. Furthermore,  $\mu_i, \mu_j$  denotes the mean pixel intensity in an  $11 \times 11$  window centered at  $(i, j)$ , while  $\sigma_i^2$  and  $\sigma_j^2$  represent the variances of the pixel values, and  $\mu_{ij}$  denotes the cross-covariance.  $c_1, c_2$ , and  $c_3$  are finite constants.

#### B. Performance Assessment

##### Accuracy@N

Accuracy@N (or Top-N Accuracy) is an indicator used to evaluate the performance of multi-category classifiers (such as text classification, image classification). It evaluates the performance by calculating the proportion of the top N predictions that correctly match the ground truth labels [21], as shown in Equation (16).

$$\text{Accuracy@N} = \frac{1}{M} \sum_{i=1}^M I(y_i \in \text{Top-N Predictions for } x_i), \quad (16)$$

where  $M$  is the total number of test samples,  $y_i$  is the true class label of the  $i$ -th sample,  $x_i$  is the  $i$ -th test sample, *Top-N Predictions for  $x_i$*  represents the top  $N$  predicted classes of the model for sample  $x_i$ ,  $I$  is an indicator function which equals 1 if  $y_i$  is among the *Top-N Predictions for  $x_i$* , and 0 otherwise. This study will employ Accuracy@1, which requires high standards that the first prediction of the model must be correct to ensure the reliability and accuracy of the model in practical applications. In addition, the characteristics of the error samples can be analyzed and the proposed model architecture can be adjusted.

##### Correlation coefficient

A set of four images with diverse levels of haze was employed in each experimental trial. We evaluate the correlation between generated and ground truth answer rankings using Pearson, Spearman, and Kendall correlation coefficients (Equations 17-19) [22].

$$r = \frac{\sum (x_i - \bar{x})(y_i - \bar{y})}{\sqrt{\sum (x_i - \bar{x})^2 \sum (y_i - \bar{y})^2}} \quad (17)$$

where  $r$  is the Pearson correlation coefficient,  $x_i$  is the  $i$ -th ranked observation value of the predicted ranking variable  $x$ , and  $y_i$  is the  $i$ -th ranked observation value of the actual ranking variable  $y$ . And  $\bar{x}$  and  $\bar{y}$  are the mean values of variable  $x$  and variable  $y$  respectively. The value  $r$  ranges from -1 to 1, with 1 indicating a perfect positive correlation,

-1 indicating a complete negative correlation, and 0 indicating no correlation.

$$\rho = 1 - \frac{6 \sum d_i^2}{n(n^2 - 1)}, \quad (18)$$

where  $\rho$  is the Spearman correlation coefficient,  $n$  is the number of all sorted samples, and  $\sum d_i^2$  is the sum of the squared differences of the sorted values of all samples. The value  $\rho$  ranges from -1 to 1, where 1 represents a completely positive monotonic relationship, -1 represents a completely negative monotonic relationship, and 0 represents no monotonic relationship.

$$\tau = \frac{2(C - D)}{n(n - 1)}, \quad (19)$$

where  $\tau$  is the Kendall correlation coefficient,  $C$  represents the number of pairs of observations where the two variables are ranked in the same order, while  $D$  represents the number of pairs where the rankings are reversed. The total number of pairs of observations is denoted by  $n$ . The value  $\tau$  ranges from -1 to 1, with 1 indicating completely consistent rankings, -1 indicating complete inconsistency, and 0 indicates no association between the rankings.

Among the three correlation coefficients, Pearson's correlation is appropriate for assessing linear relationships under the assumption of normally distributed data; however, it is highly sensitive to outliers. In contrast, Spearman's and Kendall's correlation coefficients are better suited for monotonic relationships and exhibit greater robustness to outliers. Notably, Kendall's correlation is particularly advantageous when analyzing ordinal data. In this study on haze detection, a series of experiments will be conducted to evaluate and determine the most suitable correlation coefficient for the analysis

### C. Adjust Dehaze Parameters

The performance of the model proposed in this study depends on the two key parameters of the dark channel prior dehazing algorithm: local patch size and transmission  $w$ . These parameters directly affect the extraction of haze information from hazy images, which is essential for our experiments. Therefore, under the proposed model combined with effective image quality assessment methods. We further performed a two-factor sensitivity analysis of these two parameters. By understanding the impact of parameter changes on model output results, we can obtain the most appropriate parameter values to ensure the reliability and accuracy of the model.

In summary, we use Algorithm 1 to help readers quickly review the core concepts of the proposed model to improve readability and enhance feasibility.

**Algorithm 1:** Proposed haze detection

---

**Input:** CCTV image  $J$   
**Output:** Haze degree classification

- 1 **Dark channel prior dehazing:**
- 2 Obtain dark channel image  $J^{dark}(x)$  according to Eq. (3);
- 3 Estimate atmospheric light  $A$  by finding the max brightness from the top 0.1% pixels in  $J^{dark}(x)$ ;
- 4 Calculate the transmission  $t(x)$  according to Eq. (6);
- 5 Obtain the dehazed image  $I(x)$  according to Eq. (7);

---

- 6 **Image quality assessment:**
- 7 Evaluate the values of MAE, MSE, SNR, PSNR, and SSIM;
- 8 **Performance assessment:**
- 9 Evaluate the values of Accuracy @1, Pearson, Spearman, and Kendall
- 10 **Adjust dehaze parameters:**
- 11 Obtain the optimal values of the parameters patch size and  $w$  by two-factor sensitivity analysis
- 12 Update the parameters of the model
- 13 Complete classification results

---

## IV. EXPERIMENTAL RESULTS AND DISCUSSION

### A. Haze Image Database

Currently, there are quite a few databases used in dehazing research, such as O-Haze [23], Dense-Haze [24], NH-HAZE [25], RESIDE [26], and HazeRD [27]. Most of them are a set of comparison images with and without haze, and this study must detect different haze degrees in the same scene. Therefore, in addition to referring to the IMFD [28], CHIC [29], FRIDA2 [30], and SHIA [31] databases, we also collect time-lapse images of various fixed scenes on the Internet to extract and classify the required haze images, as shown in Fig. 6. The experimental database finally collected has a total of 520 different scenes, each scene has 4 images of different haze degrees, a total of 2,080 images, and they are labeled as 4 categories: no haze, light, medium, and heavy.

### B. Experimental Environment

The experiment was carried out using Matlab R2021a programming on a Windows 11 (x64) operating system. It was executed on a PC with an Intel Core i5-11400F CPU running at 4.4GHz and 16GB of RAM.

### C. Experimental Results

#### Performance of different image quality assessment methods

To further investigate the optimal image quality assessment method for the proposed model, we conducted experiments. First, the local patch of the dark channel prior dehazing in the proposed model is  $39 \times 39$ , and the transmission parameter  $w$  is 0.997. Then for the experimental database, there are a total of 520 types of images of different scenes, each scene has 4 images of different haze degrees. We employ five different methods of MAE, MSE, SNR, PSNR, and SSIM to evaluate and sort. Finally, Accuracy@1, Pearson, Spearman, and Kendall were used as performance evaluation indicators. The experimental results are shown in Table I, and the corresponding conclusions are as follows:

- 1) It shows that the proposed model combined with the SSIM method has the optimal performance, with Accuracy@1 reaching 96.55%. In contrast, the performance of other methods such as MAE, MSE, SNR, and PSNR is significantly lower, with scores of only 28.45%, 31.90%, 30.17%, and 35.34%, respectively. This is mainly because SSIM can effectively capture the changes in luminance, contrast, and structure of haze images to distinguish different haze degrees, while MAE, MSE, SNR, and PSNR methods cannot reflect subtle image quality variations.



Fig. 6. Progressive haze severity from left to right.

2) Through the evaluation results of the correlation coefficients Pearson, Spearman, and Kendall, we can also know that SSIM is the best way to evaluate the haze degree, and its predicted ranking and ground truth ranking have the highest correlation. Both Pearson and Spearman are 0.9862, and Kendall is 0.9770. The correlation coefficient values of other MAE, MSE, SNR, and PSNR methods are roughly between 0.0345 and -0.2483, which means that there is almost no correlation between the predicted ranking and the ground truth ranking.

TABLE I  
PERFORMANCE OF THE PROPOSED MODEL UNDER DIFFERENT IMAGE QUALITY EVALUATION METHODS

Method	Metrics			
	Accuracy@1(%)	Pearson	Spearman	Kendall
MAE	28.45	-0.0828	-0.0828	-0.1034
MSE	31.90	0.0345	0.0345	0.0115
SNR	30.17	-0.2483	-0.2483	-0.1954
PSNR	35.34	-0.0345	-0.0345	-0.0115
SSIM	96.55	0.9862	0.9862	0.9770

Therefore, it is known from the above performance evaluation results that the proposed model combined with the SSIM image quality evaluation method can effectively distinguish different haze degrees and achieve the optimal performance.

**Sensitivity analysis of model parameters**

According to the conclusion of the previous subsection, the proposed model combined with the SSIM image quality assessment method has the better performance. We further conducted a two-factor sensitivity analysis on the two parameters of local patch size and transmission  $w$ . Part of the experimental results are shown in Table II, and their analysis diagrams are shown in Fig. 8. The relevant conclusions are as follows:

1) When the local patch size is between 39×39 and 47×47,

there is better accuracy, which means that this range size can better capture the darkest pixels in the image and smooth out noise in the patch. This will make the dark channel value stable and accurate, and capture haze information more effectively. Due to space constraints, only a portion of the results are shown in Fig. 7. In fact, the local patch sizes used in our experiments ranged from 3×3 to 69×69. The results demonstrate that the accuracy decreases as the patch size becomes either too small or too large. The intuitive color distribution from the heatmap in Fig. 8 also effectively presents patterns and distributions in experimental data. Therefore, selecting an appropriate size for the local patch is crucial for achieving optimal performance of our model.

TABLE II  
PARTIAL RESULTS FOR ACCURACY@1(%) IN TWO-FACTOR SENSITIVITY ANALYSIS OF LOCAL PATCH SIZE AND PARAMETER  $w$

Patch size	$w$									
	0.82	0.84	0.86	0.88	0.90	0.92	0.94	0.96	0.98	1
19×19	86.21	86.21	86.21	86.21	86.21	<b>84.48</b>	<b>84.48</b>	<b>84.48</b>	86.21	86.21
21×21	86.21	86.21	86.21	86.21	86.21	<b>84.48</b>	<b>84.48</b>	85.34	86.21	87.93
23×23	87.93	87.93	87.93	87.93	87.93	86.21	87.07	87.93	87.93	88.79
25×25	87.93	87.93	87.93	87.93	87.93	87.07	87.93	87.93	87.93	88.79
27×27	87.93	87.93	87.93	87.93	89.66	87.93	87.93	89.66	88.79	88.79
29×29	91.38	91.38	91.38	89.66	91.38	89.66	90.52	90.52	92.24	91.38
31×31	91.38	91.38	91.38	93.10	93.10	91.38	93.10	93.10	93.97	94.83
33×33	91.38	91.38	92.24	93.10	93.10	93.10	93.10	92.24	93.97	94.83
35×35	91.38	91.38	92.24	93.10	93.10	93.10	92.24	92.24	93.97	94.83
<b>37×37</b>	91.38	91.38	93.10	93.10	92.24	92.24	92.24	92.24	93.97	<b>96.55</b>
<b>39×39</b>	91.38	91.38	92.24	92.24	92.24	92.24	92.24	92.24	94.83	<b>96.55</b>
<b>41×41</b>	91.38	92.24	92.24	92.24	92.24	92.24	92.24	92.24	94.83	<b>96.55</b>
<b>43×43</b>	91.38	92.24	92.24	92.24	92.24	90.52	92.24	93.10	93.10	<b>96.55</b>
<b>45×45</b>	90.52	92.24	92.24	92.24	92.24	90.52	92.24	93.10	93.10	<b>96.55</b>
<b>47×47</b>	90.52	92.24	92.24	92.24	92.24	90.52	93.10	93.10	93.10	<b>96.55</b>
49×49	87.07	90.52	90.52	90.52	90.52	91.38	91.38	93.10	93.10	94.83
51×51	87.07	90.52	90.52	90.52	91.38	91.38	93.10	93.10	93.10	94.83

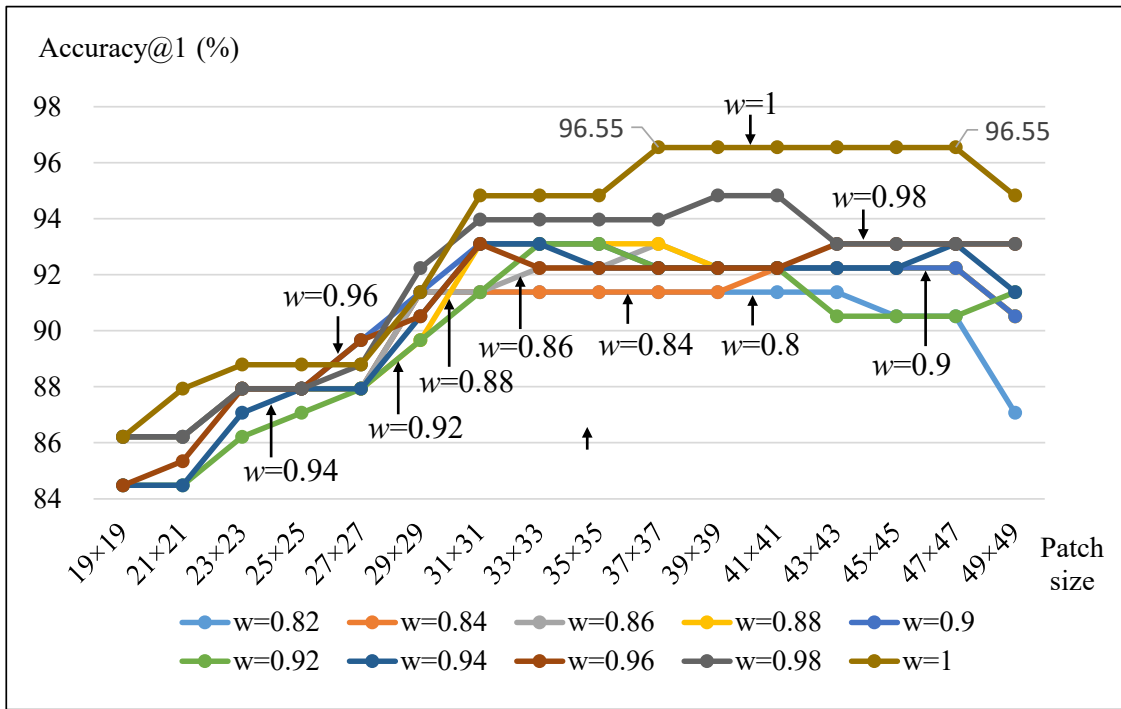


Fig. 7. Accuracy@1 trends with varying local patch size and parameter  $w$ .

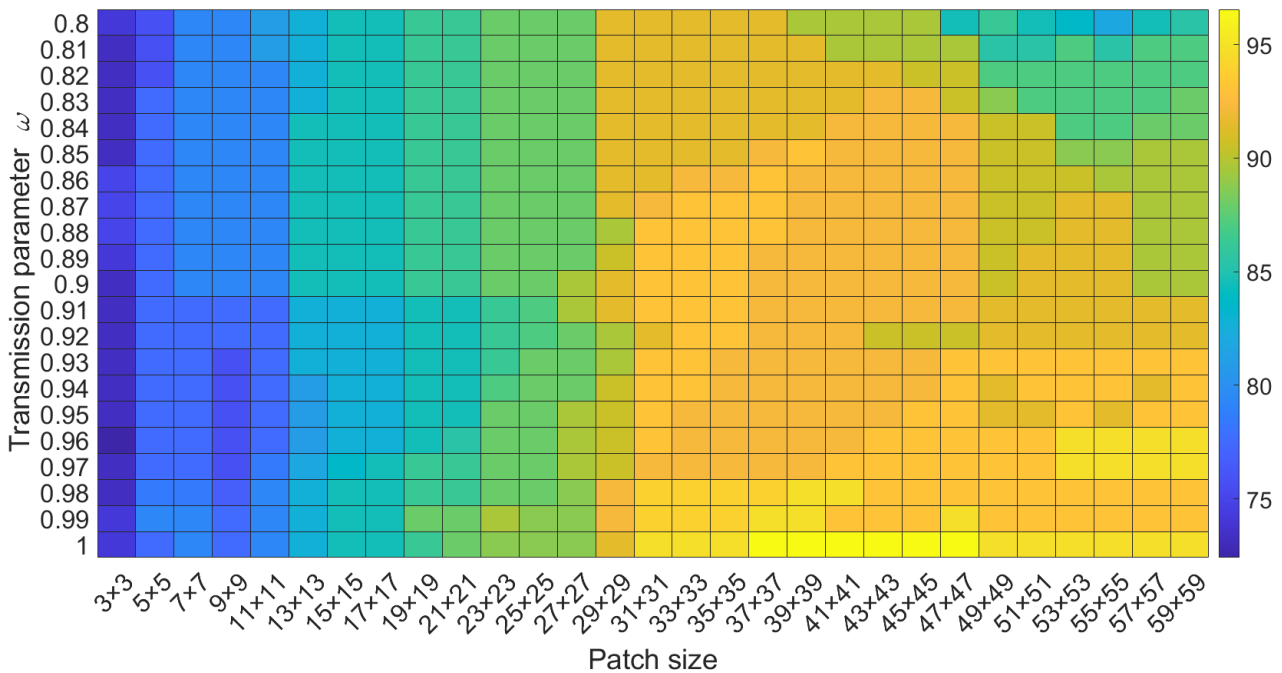


Fig. 8. Performance heatmap for local patch size and parameter  $w$

2) When  $w=1$ , there is better accuracy, that is, the parameter  $w$  in equation (6) is removed, which represents a higher transmission estimate. This allows more haze in the image to be effectively removed, and the removed haze improves the haze detection performance of the proposed model.

**Verification using the CHIC image database with haze levels**

CHIC [29] is an image database with haze levels. In the CHIC\_Static\_Scenes subset, there are two indoor scenes A and B in controlled environment. Each scene consists of 10 images with different haze densities, ranging from heavy at

level 1 to none at level 10.

Based on the model proposed in this study combined with SSIM image quality assessment, we use the two scene images A and B for example verification. The results are shown in Table III. Observing the SSIM values of these two scenes A and B under different haze densities from level 1 to level 10, it is demonstrated that the higher the haze density, the smaller the SSIM value. The results show that the model proposed in this study can indeed detect different haze densities correctly, reflecting the robustness of our model. Therefore, in practical applications, we can set SSIM thresholds for different scenes to distinguish haze levels, such as heavy, medium, thin, and no haze levels.

TABLE III

SSIM COMPARISON UNDER HAZE DENSITY LEVELS 1 TO 10 FOR SCENES A AND B IN THE CHIC IMAGE DATABASE

Scene	SSIM				
	Level 1	Level 2	Level 3	Level 4	Level 5
A	0.8495	0.8747	0.8997	0.9129	0.9407
	0.9570	0.9662	0.9801	0.9869	0.9909
B	0.8539	0.8661	0.8757	0.8821	0.9149
	0.9377	0.9382	0.9644	0.9816	0.9942

### Performance of nighttime haze image detection

Dehazing nighttime haze images is a specialized research topic [32-38], so we collected a dataset of nighttime haze images from publicly available dataset to verify the performance of our proposed model in nighttime conditions. Since these datasets all use daytime haze images to simulate or convert them into nighttime scenes, except for RealNightHaze [35, 38] which collects 440 haze images at real nighttime, it does not have many images of different haze density in a single scene. Finally, 340 different scenes were collected, each with 4 images of different haze densities, totaling 1,360 images, as shown in Fig. 9.

Then we also use five different methods, including MAE, MSE, SNR, PSNR, and SSIM, for calculation and ranking, and finally use Accuracy@1, Pearson, Spearman, and Kendall as performance evaluation indicators. The results are the same as those of the previous experiments using daytime haze images. The proposed model combined with the SSIM method has better performance, with Accuracy@1 reaching 91.67%, while the performance of other MAE, MSE, SNR, and PSNR methods is very poor. Through the evaluation results of the correlation coefficients Pearson, Spearman, and Kendall, we can also know that SSIM is a better method for evaluating the degree of haze, and its prediction ranking has the highest correlation with the ground truth ranking. Pearson and Spearman are both 0.9862, and Kendall is 0.9770, as

shown in Table IV.

In addition, we believe that this experiment is an exploratory analysis because the nighttime haze image dataset used was obtained through simulation or conversion. In the future, we will configure additional light sources in night environments and build our own database of nighttime haze images in real scenarios. This overcomes research limitations and ensures the quality and reliability of this research result.

TABLE IV

SSIM-BASED EVALUATION OF THE PROPOSED MODEL FOR NIGHTTIME HAZE IMAGE DETECTION

Method	Metrics			
	Accuracy@1(%)	Pearson	Spearman	Kendall
SSIM	91.67	0.9667	0.9667	0.9444

### V. CONCLUSION

In order to apply image processing technology to existing CCTV systems used in traffic for haze detection, this study proposes a haze detection model. The proposed model employs the dark channel prior dehazing algorithm to process original CCTV images, followed by a comparative evaluation of the dehazed and original images using image quality assessment metrics. Then the haze degree of the image is judged based on the assessment results. Experimental results show that, whether it is a haze image during the day or at night, that the proposed model combined with the SSIM image quality assessment method can reflect the changes in brightness, contrast, and structure of haze images, thereby distinguishing different haze degrees. In addition, we also used the correlation coefficients Pearson, Spearman, and Kendall to once again prove that SSIM has the highest correlation between the haze degree calculation and ranking results and the actual ranking. Finally, the proposed model performs sensitivity analysis on the local patch size and transmission parameter  $w$  to obtain better parameter values.



Fig. 9. Progressive nighttime haze density from left to right.

In the future, the haze detection model proposed in this study has the potential to be deeply integrated with the intelligent transportation system (ITS) architecture. This model can not only be applied to existing CCTV infrastructure for smog level monitoring, but can also further cooperate with other ITS modules, such as intelligent traffic lights, traffic flow control and intelligent navigation systems. In the next phase of research, we will overcome the haze environment at night by configuring additional lighting or sensors to ensure full-time detection and improve the service availability of the model.

## REFERENCES

- [1] S.-F. Wang, "The dense fog detector on National Highway 65 will alert if the visibility is less than 400 meter," *Central News Agency*, 2023/3/3. <https://www.cna.com.tw/news/ahel/202303030193.aspx> (accessed 20 May 2024)
- [2] Real-time traffic conditions, highway 1968. <https://1968.freeway.gov.tw/roadcctv> (accessed 17 Feb. 2024)
- [3] Z. Wei, J. Xu, S. Wang, S. Liu, S. Qiu, "Nighttime visual recognition performance of light emitting diode traffic signs," *Canadian Journal of Civil Engineering*, vol. 47, no. 9, pp1050-1058, 2019.
- [4] F. Guo, J. Yang, Z. Liu, J. Tang, "Haze removal for single image: A comprehensive review," *Neurocomputing*, vol. 537, pp85-109, 2023.
- [5] K. He, J. Sun, X. Tang, "Single image haze removal using dark channel prior," *IEEE Transactions on Pattern Analysis and Machine Intelligence*, vol. 33, no. 12, pp2341-2353, 2011.
- [6] Q.-C. Zheng, Z.-D. Zhang, J.-G. Liu, P.-H. Zhu, W.-P. Ma, "Welding seam image dust removal algorithm based on fusion of dual-scale dark channel and bright channel," *IAENG International Journal of Computer Science*, vol. 48, no. 2, pp277-284, 2021.
- [7] G. Guo, H. Lv, Y. Zhao, H. Liu, Y. Zhang, "An event-guided image motion deblurring method based on dark channel prior loss," *Optics and Lasers in Engineering*, vol. 181, 2024.
- [8] G. Hou, J. Li, G. Wang, H. Yang, B. Huang, Z. Pan, "A novel dark channel prior guided variational framework for underwater image restoration," *Journal of Visual Communication and Image Representation*, vol. 66, 2020.
- [9] R. T. Tan, "Visibility in bad weather from a single image," *2008 IEEE Conference on Computer Vision and Pattern Recognition (CVPR)*, 2008.
- [10] Q. Zhu, J. Mai, L. Shao, "A fast single image haze removal algorithm using color attenuation prior," *IEEE Transactions on Image Processing*, vol. 24, no. 11, pp3522-3533, 2015.
- [11] K. Tang, J. Yang, J. Wang, "Investigating haze-relevant features in a learning framework for image dehazing," *IEEE Conference on Computer Vision and Pattern Recognition*, pp2995-3000, 2014.
- [12] C.-S. Fuh, T.-C. Tung, "MCPA: A fast single image haze removal method based on the minimum channel and patchless approach," *IEEE Access*, 2022.
- [13] B. Cai, X. Xu, K. Jia, C. Qing, D. Tao, "Dehazenet: An end-to-end system for single image haze removal," *IEEE Transactions on Image Processing*, vol. 25, no. 11, pp5187-5198, 2016.
- [14] C.-H. Yeh, C.-H. Huang, L.-W. Kang, "Multi-scale deep residual learning-based single image haze removal via image decomposition," *IEEE Transactions on Image Processing*, vol. 29, pp3153-3167, 2019.
- [15] Z. Chen, Z. He, Z.-M. Lu, "DEA-Net: Single image dehazing based on detail-enhanced convolution and content-guided attention," *IEEE Transactions on Image Processing*, vol. 33, pp1002-1015, 2024.
- [16] E. J. McCartney, *Optics of the atmosphere: scattering by molecules and particles*, New York, John Wiley and Sons, 1976.
- [17] G. James, D. Witten, T. Hastie, R. Tibshirani. *An Introduction to Statistical Learning: with Applications in R (2nd edition)*, Springer, 2021.
- [18] B. T. Bosworth, W. R. Bernecky, J. D. Nickila, B. Adal, "Estimating signal-to-noise ratio (SNR)," *IEEE Journal of Oceanic Engineering*, vol. 33, no. 4, pp414-418, 2008.
- [19] A. Hore, D. Ziou, "Image quality metrics: PSNR vs. SSIM," *International Conference on Pattern Recognition*, pp2366-2369, 2010.
- [20] Z. Wang, A. C. Bovik, H. R. Sheikh, E. P. Simoncelli, "Image quality assessment: from error visibility to structural similarity," *IEEE Transactions on Image Processing*, vol. 13, no. 4, pp600-612, 2004.
- [21] T.-Y. Liu, *Learning to Rank for Information Retrieval*, Springer, 2011.
- [22] M. Kendall, J. D. Gibbons, *Rank Correlation Methods (5th Edition)*, Edward Arnold, London, 1990.
- [23] C. O. Ancuti, C. Ancuti, R. Timofte, C. De Vleeschouwer, "O-haze: a dehazing benchmark with real hazy and haze-free outdoor images," *IEEE Conference on Computer Vision and Pattern Recognition Workshops*, pp754-762, 2018.
- [24] C. O. Ancuti, C. Ancuti, R. Timofte, L. V. Gool, L. Zhang, M.-H. Yang, "Ntire 2019 image dehazing challenge report," *IEEE/CVF Conference on Computer Vision and Pattern Recognition Workshops (CVPRW)*, 2019.
- [25] C. O. Ancuti, C. Ancuti, Radu Timofte, "NH-HAZE: an image dehazing benchmark with non-homogeneous hazy and haze-free images," *IEEE/CVF Conference on Computer Vision and Pattern Recognition Workshops (CVPRW)*, 2020.
- [26] B. Li, W. Ren, D. Fu, D. Tao, D. Feng, W. Zeng, Z.-Y. Wang, "Benchmarking single-image dehazing and beyond," *IEEE Transactions on Image Processing*, vol.28, no. 1, pp492-505, 2019.
- [27] Y. Zhang, L. Ding, G. Sharma, "HazeRD: an outdoor scene dataset and benchmark for single image dehazing," *IEEE International Conference on Image Processing (ICIP)*, pp3205-3209, 2017.
- [28] B. Çetinkaya, Y. Çımtay, F. N. Günay, G. N. Yılmaz, "A new multi-level hazy image and video dataset for benchmark of dehazing methods," *Fourth International Conference on Image Processing and Capsule Networks*, pp269-280, 2023.
- [29] J. E. Khoury, J.-B. Thomas, A. Mansouri, "A database with reference for image dehazing evaluation," *Journal of Imaging Science and Technology*, vol. 62, no. 1, 2018.
- [30] J.-P. Tarel, N. Hautière, L. Caraffa, A. Cord, H. Halmaoui, D. Gruyer, "Vision enhancement in homogeneous and heterogeneous fog," *IEEE Intelligent Transportation Systems Magazine*, vol. 4, no. 2, pp6-20, 2012.
- [31] J. E. Khoury, J.-B. Thomas, A. Mansouri, "A spectral hazy image database," *Image and Signal Processing: 9th International Conference (ICISP)*, pp44-53, 2020.
- [32] S.-C. Pei, T.-Y. Lee, "Nighttime haze removal using color transfer pre-processing and dark channel prior," In *2012 19th IEEE International Conference on Image Processing*, pp957-960, 2012.
- [33] Y. Li, R. T. Tan, M. S. Brown, "Nighttime haze removal with glow and multiple light colors," In *Proceedings of the IEEE International Conference on Computer Vision*, pp226-234, 2015.
- [34] J. Zhang, Y. Cao, S. Fang, Y. Kang, C.-W. Chen, "Fast haze removal for nighttime image using maximum reflectance prior," In *Proceedings of the IEEE Conference on Computer Vision and Pattern Recognition*, pp7418-7426, 2017.
- [35] J. Zhang, Y. Cao, Z.-J. Zha, D.-C. Tao, "Nighttime dehazing with a synthetic benchmark," In *Proceedings of the 28th ACM International Conference on Multimedia*, pp2355-2363, 2020.
- [36] S. Hong, M. Kim, H. Lee, "Nighttime single image dehazing based on the structural patch decomposition," *IEEE Access*, vol. 9, 2021.
- [37] Z.-Y. Jin, H.-J. Feng, Z.-H. Xu, Y.-T. Chen, "Nighttime image dehazing by render," *Journal of Imaging*, vol. 9, no. 8, 2023.
- [38] Y. Jin, B. Lin, W. Yan, Y. Yuan, W. Ye, R. T. Tan, "Enhancing visibility in nighttime haze images using guided APSF and gradient adaptive convolution," In *Proceedings of the 31st ACM International Conference on Multimedia*, pp2446-2457, 2023.